2012 SCEC Report

Validation of lateral reflectors in southern California using time reversal seismic imaging

Principal Investigator:
Carl Tape
Assistant Professor of Geophysics
University of Alaska Fairbanks
Geophysical Institute
903 Koyukuk Dr., Fairbanks, AK, 99775
carltape@gi.alaska.edu // 907-474-5456

2011 SCEC RFP

Proposal Categories:	B: Integration and Theory
Interdisciplinary Focus Areas:	Unified Structural Representation
	Ground Motion Prediction
Science Objectives:	B4, B3, C

Motivation and summary

Each earthquake in southern California generates some waveforms that cannot be adequately modeled by current techniques. The limitation lies not with numerical techniques, which can be scaled to nearly arbitrarily high frequencies (e.g., *Carrington et al.*, 2008), but rather with our representation of the seismic structure. In this investigation we focus on waveforms that arrive at stations *after* the direct surface waves. If our structural model and numerical technique can accurately simulate these coda waveforms, then we open the door to using additional waveforms for seismological investigations of source and structure.

In this investigation we developed and applied two tools to facilitate a search for laterally reflected surface waves in southern California: (1) seismic imaging with impedence sensitivity kernels ("imaging kernels") and (2) polarization analysis of three-component waveforms. The target bandpass for the waveforms in this investigation was 3–10 s, which are very short periods for modeling full waveforms in the southern California network. The imaging kernels provide a potentially unbiased means for illuminating reflectors; however, we found that considerable care must be taken in selecting the observed waveforms, in order to generate interpretable images. We performed a polarization analysis using `threecomp`, a new extension of the Waveform Suite Matlab toolbox (*Reyes and West*, 2011). This provides an invaluable tool for visualizing three-component seismograms and for identifying complex seismic phases. We document several of the most promising reflectors in southern California; however, unequivocal proof of these reflectors will require further study and possibly denser station coverage.

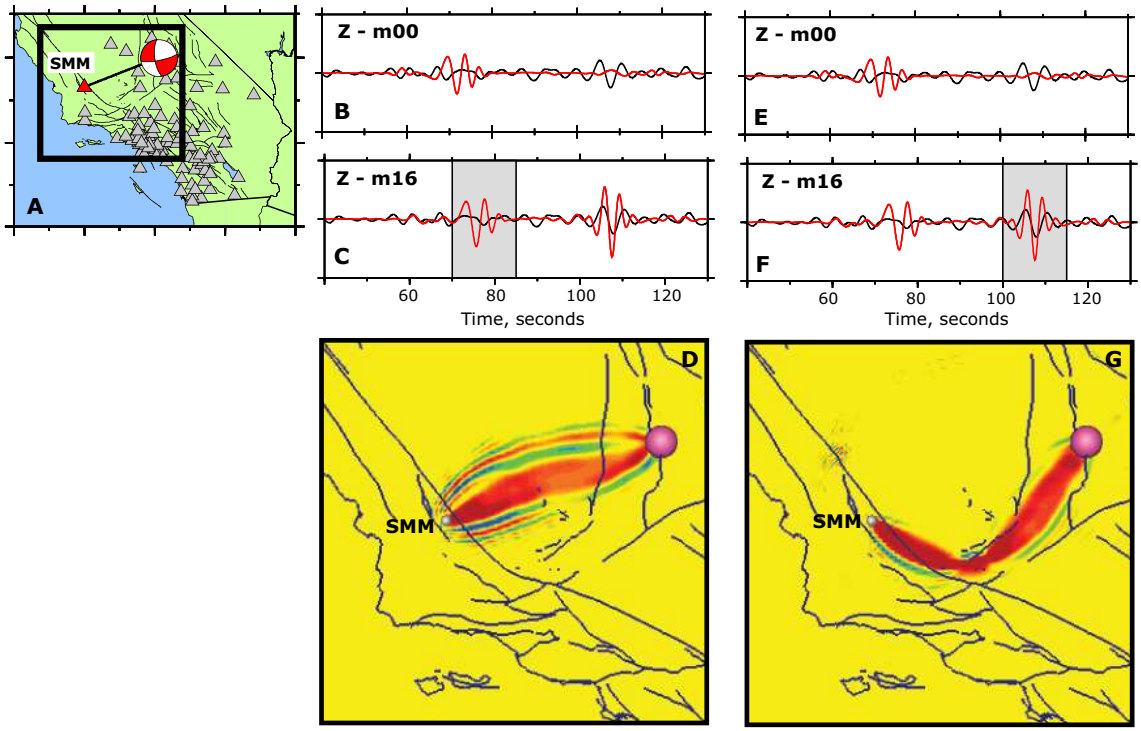

Figure 1: Reflected Rayleigh wave at the Tehachapi Mountains. The time windows shown in (c) and (f) highlight two different surface waves. All seismograms are filtered in the period range 3–30 s. (a) Map showing earthquake source (10992159) and station coverage. (b) Data (black) and $\mathbf{m}_{00}$ 3D synthetics (red). (c) Data (black) and $\mathbf{m}_{16}$ 3D synthetics (red). Synthetic waveform within the time window follows the propagation path shown in (d). (d) Horizontal cross section at 4 km depth of a volumetric sensitivity kernel corresponding to the windowed synthetic waveform in (c). The path illuminates the "direct" Rayleigh wave, though the path does not lie on the great circle between source and station. (e)–(g) Same as (b)–(d), but highlighting the second time window, which is only apparent in the $\mathbf{m}_{16}$ synthetics.

Laterally reflected surface waves

Laterally reflected surface waves have been studied from a theoretical perspective for decades, but there have been relatively few observational studies (*Snieder*, 1988; *Ji et al.*, 2005; *Stich and Morelli*, 2007). For southern California earthquakes there are numerous examples of high signal-to-noise waveforms that arrive after the main surface wave arrival (e.g., Figure 3)—we will refer to these waveforms generically as "coda waveforms." In exceptional cases, these coda waveforms are even larger than the primary waveforms (Figure 1).

We are able to generate some laterally reflected—or strongly refracted—surface waves in synthetic seismograms. Figure 1 shows data-vs-synthetics for the displacement vertical component of a seismogram, comparing synthetics for an initial 3D reference model with those of the iteratively improved 3D model ($\mathbf{m}_{16}$: *Tape et al.*, 2009, 2010a). While coda waveforms of $\mathbf{m}_{16}$ synthetics resemble coda waveforms in the data (in amplitude, duration, frequency content), there are few examples among tens of thousands of comparisons that show unequivocal agreement. Our study attempts to isolate the responsible reflectors in tandem with their manifestations as coda waveforms.

We select a set of 32 earthquakes and 83 stations for this study, corresponding to a maximum of 7968 seismograms (Z,E,N). The stations near the major sedimentary basins are avoided, since they are dominated by multiple reflections of the resonating basins. The earthquakes are selected from the reference set of 234 from *Tape et al.* (2010a) that will be used as part of a larger validation data set to assess future improvements to CVM-H 6.3.

Imaging kernels derived from coda waveforms

We use time reversal imaging to illuminate potential reflectors in southern California. Time reversal imaging has been used recently to identify the Apennines in Italy as a prominent reflector of surface waves (*Stich and Morelli*, 2007; *Stich et al.*, 2009). The technique benefits from the accuracies of the forward simulations of the seismic wavefield, which are performed using the spectral-element method (SEM) (*Komatitsch and Vilotte*, 1998; *Komatitsch et al.*, 2004). We use `SPECFEM3D` for the wavefield simulations as well as for the imaging (*Liu and Tromp*, 2006). We follow the approach of *Stich et al.* (2009) but use much shorter period seismic waveforms (3–10 s), which are sensitive to structure in the uppermost 10 km of the crust. The technique requires a smooth background model, which we obtain by smoothing model $\mathbf{m}_{16}$ (*Tape et al.*, 2009) with a Gaussian function (12 km horizontal, 2 km vertical). The smoothing has the effect of suppressing synthetic waveforms that are associated with reflections (single and multiple).

In principle one could simply time-reverse all coda waveforms for all events and all stations, then stack the individual "event kernels" to get a composite image of the dominant reflectors (*Stich et al.*, 2009). However, we found that there is too much complexity in the 3–10 s coda waveforms of southern California for this approach to work: the "unbiased" event kernels generally have little interpretable pattern and are dominated by noise. Additional user bias can be imposed by selecting only specific events, specific stations, or specific waveforms. But even in this restrictive, trial-and-error approach, it is challenging to obtain easily interpretable sensitivity kernel. (In the extreme case, even one waveform for one station can create a complicated kernel with scattering fringes in multiple regions.)

Based on a targeted trial-and-error analysis with approximately 100 simulations, we have identified lateral reflectors in proximity to: the southernmost San Joaquin basin, the Los Angeles basin, the San Pedro basin, the Ventura basin, the Manix basin, the San Clemente–Santa Cruz–Santa Barbara ridge, and isolated segments of the San Jacinto and San Andreas faults (*Tape et al.*, 2010b,c). The correspondence between observed coherent coda waveforms and the imaged reflectors provides a solid basis for interpreting the kernel features as material contrasts. However, because artifacts can easily arise in such high-frequency simulations, a more detailed investigation is needed to bridge the gap from kernel feature to material contrast.

Here we document three challenges associated with time-reversal imaging of these coda wave-

forms. First and foremost, many—arguably, most—of the coda waveforms arise from multiple reflections associated with resonance from sedimentary basins. These waveforms ought to be avoided, since the imaging technique will accurately illuminate single reflectors only; each oscillation of a basin will create a coda waveform that will "pick off" a different section of the forward wavefield when making the imaging kernel. Second, there is substantial variability in the amplitude of the coda waveforms that is due to the source radiation pattern. Some remedies for correcting for this effect were presented in *Danecek et al.* (2011). Third, the forward wavefield will contain some spurious reflections from imperfect boundaries; the coda waveforms may illuminate the spurious sensitivities of these paths. Care must be taken to suppress the boundary reflections, or one can use a larger simulation region (computationally expensive), or one can manually check that the observed coda time windows do not contain any synthetic waveforms from spurious reflections.

Polarization analysis

Polarization analysis is an essential tool for analyzing directivity of surface waves from earthquakes or ambient noise (*Vidale*, 1986; *Laske et al.*, 1994; *Ji et al.*, 2005; *Tanimoto and Alvizuri*, 2006). We performed a polarization analysis of all 32 events using the Waveform Suite, a Matlab toolbox developed by *Reyes and West* (2011). This provides a direct means for visualizing three-component ground motion by distilling the time-dependent covariance matrix $\mathbf{C}(t)$ into interpretable, time-dependent, scalar quantities: the energy of the signal, the azimuth and inclination of the principal eigenvector of $\mathbf{C}$, and the rectilinearity and planarity of the motion (e.g., *Montalbetti and Kanasewich*, 1970). For example, a P wave has high rectilinearity and potentially high inclination, a Love wave has high rectilinearity and low inclination, a Rayleigh wave has low rectilinearity and high planarity. Two examples are shown in Figures 2 and 3. Figure 2 highlights a coda waveform, visible on all three components, that results in a maximal peak in energy. The drop in rectilinearity and change in both azimuth and inclination suggest a distinct seismic phase, which in this case is likely a reflected Rayleigh wave. Figure 3 highlights a probably coda Rayleigh wave with high planarity, low rectilinearity, and deviations of azimuth and inclination.

Though it provides a computationally inexpensive and important perspective on ground motion, polarization analysis presents several challenges, especially at the relatively short periods of interest (3–10 s). First, there are often multiple arrivals of seismic phases at any given time; the polarization analysis will return the "averaged" motion of these arrivals, whereas you are interested in extracting distinct signatures of (surface or body) waves. (Note that the kernel-based imaging technique does not have this limitation; it will illuminate all potential reflectors that could be responsible for a composite waveform.) Second, seismic noise, such as before the origin time of the earthquake, exhibits covariance that is comparable to some of the high-amplitude "signal" waveforms. Seismic phases should only be interpreted when there is a combination of high enough energy in the waveforms, high enough signal-to-noise (noise as measured before the origin time), and high enough rectilinearity or planarity of the signal (*Ereditato and Luongo*, 1994).

Future work

Our future efforts will encompass a quantitative, comprehensive polarization analysis for all 234 earthquakes. This will provide some insights into the extreme complexity of these coda waveforms. Furthermore we will test the polarization analysis on different data sets: socal1D synthetics, with or without realistic noise, and socal3D synthetics, with or without noise. We would also like to perform the analysis with denser arrays with 5 km station spacing. The station spacing in the southern California network is at the limit of being able to resolve the target features. (For example, there are no nearby stations in Figure 1 to test for waveform coherence.) The current station spacing is better suited for examining longer period coda waveforms (*Stich et al.*, 2009), which would target lower crustal reflectors rather than the basin-boundary scales of the uppermost 10 km.

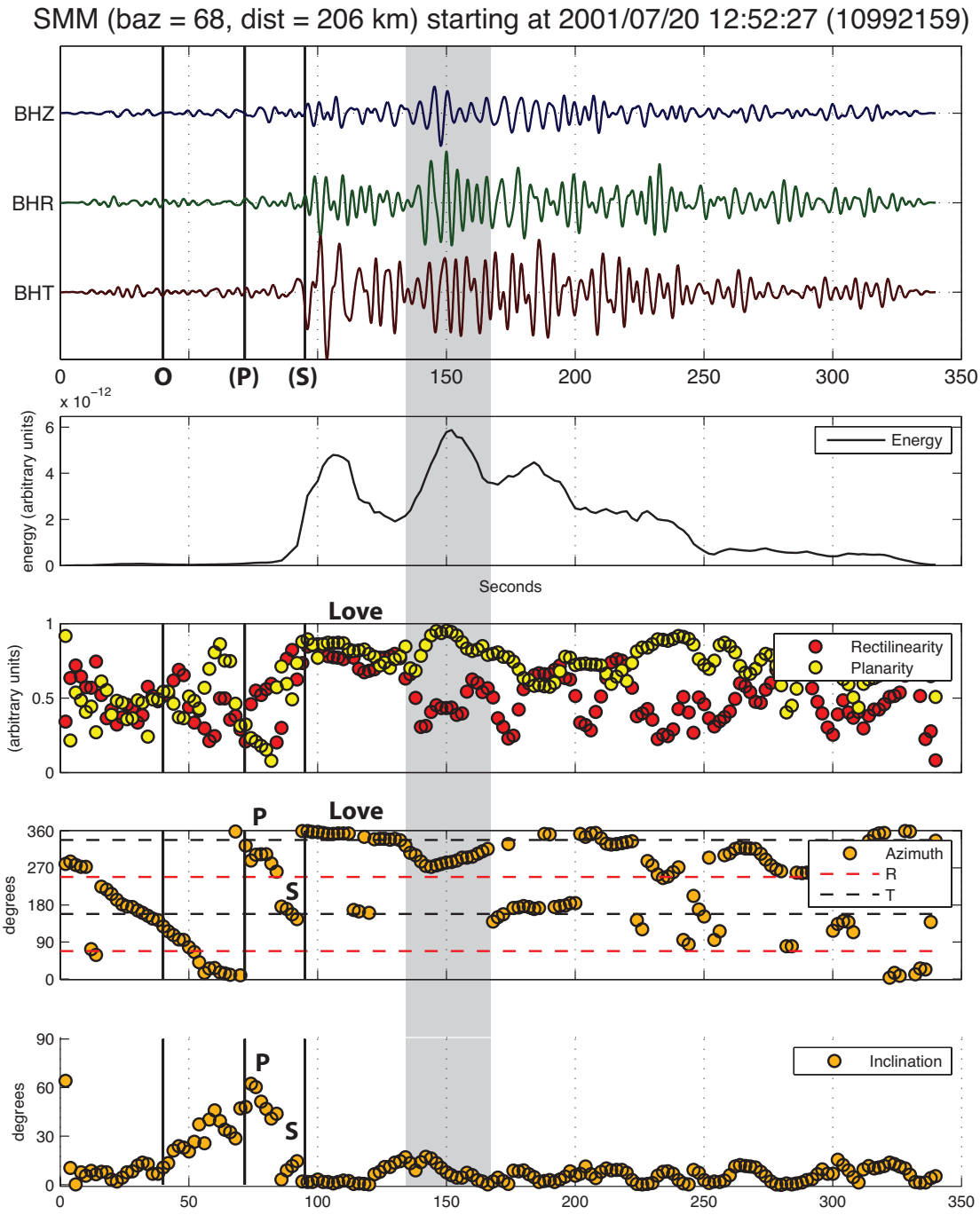

Figure 2: Example plot of polarization analysis for one station for one event for a very complicated seismogram. See Figure 1 for source-station geometry. The three-component recorded seismogram is shown as Z-R-T components, filtered 3–10 s. The vertical lines correspond to the origin time, the predicted P arrival time (for a 1D model), and the predicted S arrival time. The polarization analysis distills the three-component seismogram into five scalar functions: energy, rectilinearity and planarity, azimuth, and inclination. The labels "P," "S," and "Love" denote my interpretations; the shaded time window represents the interpreted Rayleigh wave arrival highlighted in Figure 1g.

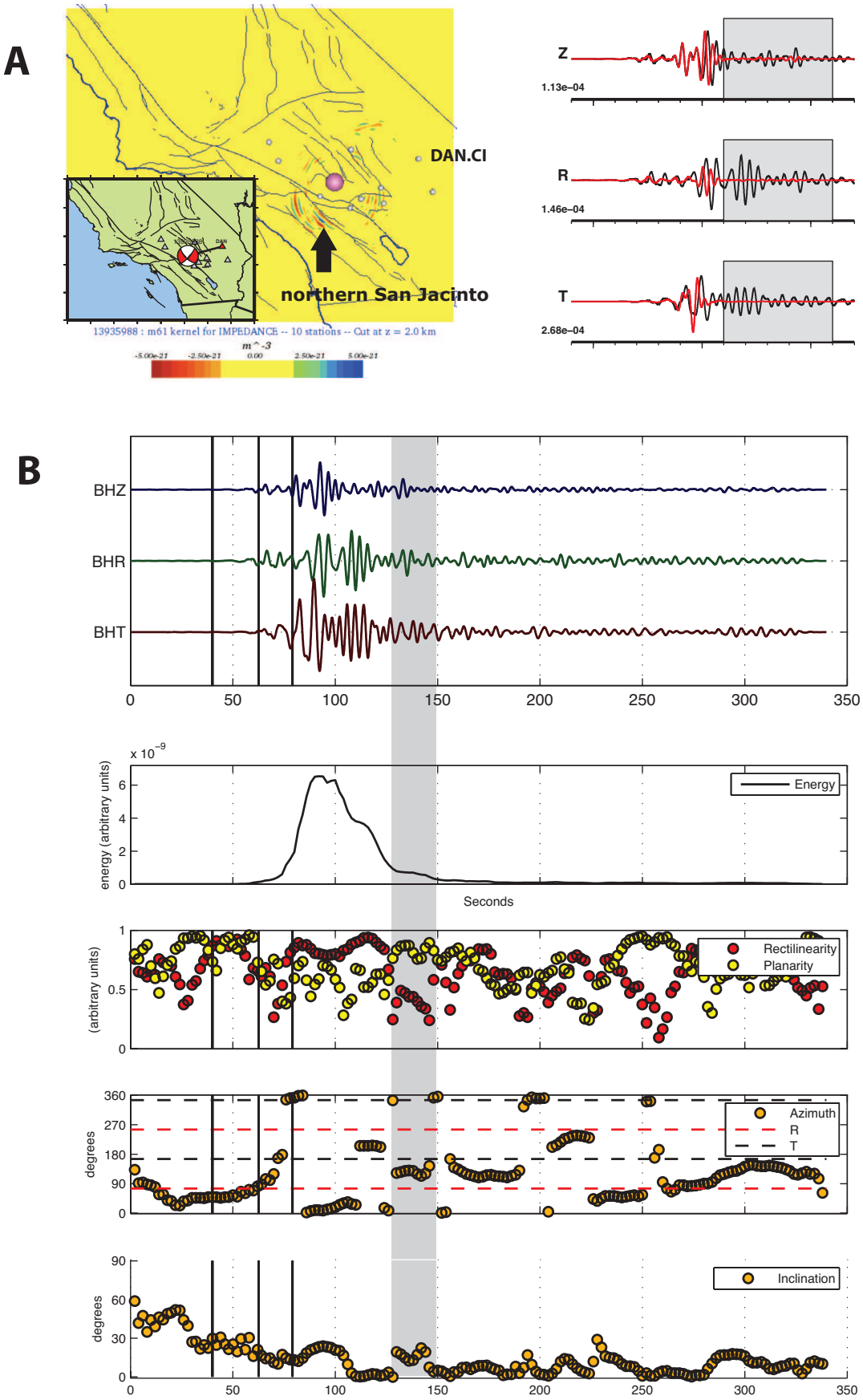

Figure 3: Composite representation of an impedance kernel (a) and a polarization analysis of one of the stations used in constructing the kernel (b). See text for details.

References

Carrington, L., D. Komatitsch, M. Laurenzano, M. M. Tikir, D. Michéa, N. Le Goff, A. Snavely, and J. Tromp (2008), High-frequency simulations of global seismic wave propagation using SPECFEM3D_GLOBE on 62K processors, in *International Conference for High Performance Computing, Storage, and Analysis (SC 2008)*, IEEE, doi:10.1109/SC.2008.5215501.

Danecek, P., D. Stich, and A. Morelli (2011), Images of the Iberian lithosphere from one local earthquake, *Bull. Seis. Soc. Am.*, *101*(2), 881–887.

Ereditato, D., and G. Luongo (1994), Volcanic tremor wave field during quiescent and eruptive activity at Mt. Etna (Sicily), *J. Volcan. Geothermal Res.*, *61*, 239–251.

Ji, C., S. Tsuboi, D. Komatitsch, and J. Tromp (2005), Rayleigh-wave multipathing along the west coast of North America, *Bull. Seis. Soc. Am.*, *95*(6), 2115–2124.

Komatitsch, D., and J.-P. Vilotte (1998), The spectral element method: An efficient tool to simulate the seismic response of 2D and 3D geological structures, *Bull. Seis. Soc. Am.*, *88*(2), 368–392.

Komatitsch, D., Q. Liu, J. Tromp, P. Süss, C. Stidham, and J. H. Shaw (2004), Simulations of ground motion in the Los Angeles basin based upon the spectral-element method, *Bull. Seis. Soc. Am.*, *94*(1), 187–206.

Laske, G., G. Masters, and W. Zürn (1994), Frequency-dependent polarization measurements of long-period surface waves and their implications for global phase-velocity maps, *Phys. Earth Planet. Inter.*, *84*, 111–137.

Liu, Q., and J. Tromp (2006), Finite-frequency kernels based on adjoint methods, *Bull. Seis. Soc. Am.*, *96*(6), 2383–2397.

Montalbetti, J. F., and E. R. Kanasewich (1970), Enhancement of teleseismic body phases with a polarization filter, *Geophys. J. R. Astron. Soc.*, *21*, 119–129.

Reyes, C. G., and M. E. West (2011), The Waveform Suite: A robust platform for manipulating waveforms in MATLAB, *Seis. Res. Lett.*, *82*, 104–110.

Snieder, R. (1988), Large-scale waveform inversions of surface waves for lateral heterogeneity 2. Application to surface waves in Europe and the Mediterranean, *J. Geophys. Res.*, *93*(B10), 12,067–12,080.

Stich, D., and A. Morelli (2007), Reflection of seismic surface waves at the northern Apennines, *Earth Planet. Sci. Lett.*, *259*, 149–158.

Stich, D., P. Danecek, A. Morelli, and J. Tromp (2009), Imaging lateral heterogeneity in the northern Apennines from time reversal of reflected surface waves, *Geophys. J. Int.*, *177*, 543–554.

Tanimoto, T., and C. Alvizuri (2006), Inversion of the HZ ratio of microseisms for S-wave velocity in the crust, *Geophys. J. Int.*, *165*, 323–335.

Tape, C., Q. Liu, A. Maggi, and J. Tromp (2009), Adjoint tomography of the southern California crust, *Science*, *325*, 988–992.

Tape, C., Q. Liu, A. Maggi, and J. Tromp (2010a), Seismic tomography of the southern California crust based on spectral-element and adjoint methods, *Geophys. J. Int.*, *180*, 433–462.

Tape, C., Q. Liu, J. Tromp, A. Plesch, and J. H. Shaw (2010b), Time reversal seismic imaging using laterally reflected surface waves in southern California, in *2010 Southern California Earthquake Center Annual Meeting, Proceedings and Abstracts*, vol. 20, p. 282.

Tape, C., Q. Liu, J. Tromp, A. Plesch, and J. H. Shaw (2010c), Time reversal seismic imaging using laterally reflected surface waves in southern California, Abstract S44A-03 presented at 2010 Fall Meeting, AGU, San Francisco, Calif., 13-17 Dec.

Vidale, J. E. (1986), Complex polarization analysis of particle motion, *Bull. Seis. Soc. Am.*, *76*, 1393–1405.

Summary of SCEC3 research highlights (Carl Tape)

1. **Adjoint tomography with CVM-H.** My PhD thesis involved performing an adjoint-based tomographic inversion with the SCEC CVM-H model (*Tape et al.*, 2009a, 2010a). This produced a model for California that is validated with tens of thousands of full waveforms from 234 high-quality crustal earthquakes. The success of the investigation was due in part to the quality of the three-dimensional reference model provided by SCEC (CVM-H). The investigation was notable both for the application of a new technique at a large scale (adjoint tomography) and for the final product, an improved tomographic model for southern California. The results were used to improve the crustal domain—above the Moho, but below the basement—in CVM-H (*Plesch et al.*, 2009)

2. **CVM-H development**. My NSF postdoctoral fellowship to Harvard allowed for close collaboration with John Shaw and Andreas Plesch in developing and testing CVM-H (*Plesch et al.*, 2009; *Tape et al.*, 2010b; *Plesch et al.*, 2011; *Tape et al.*, 2012).

3. **Static displacement fields computed using seismic wavefield simulations.** This project was begun in the final year of SCEC3. In collaboration with Brendan Meade and Jack Loveless (*Tape et al.*, 2011a), we are currently benchmarking static offset displacement fields using seismic wavefield simulations. The objective is to use static displacement fields derived from CVM-H, which is a natural extension of the currently functioning codes. These 3D Green's functions should allow for improved modeling of coseismic and interseismic processes.

4. **Estimating velocity fields and strain-rate fields.** *Tape et al.* (2009b) presented a technique for estimating continuous spatial velocity fields on the sphere by using spherical wavelet basis functions. The estimated velocity fields could then be used to directly obtain a strain-rate field. The technique was demonstrated on a 3D continuous GPS velocity field for southern California; the results were used within the SCEC comparative study of *Sandwell et al.* (2010).

Journal publications partially supported by SCEC3 funds:

- *Tape et al.* (2009a, 2010a) (Tromp)
- *Tape et al.* (2012) (Shaw)
- *Krishnan et al.* (2012) (Krishnan)

Abstract publications partially supported by SCEC3 funds:

- *Plesch et al.* (2009); *Tape et al.* (2009c, 2010c,b); *Sandwell et al.* (2010); *Tape et al.* (2010d, 2011b,a); *Plesch et al.* (2011)

References

Krishnan, S., et al. (2012), Rapid estimation of damage to tall buildings using near real-time earthquake and archived structural simulations, *Bull. Seis. Soc. Am.* (in review).

Plesch, A., C. Tape, J. H. Shaw, and members of the USR working group (2009), CVM-H 6.0: Inversion integration, the San Joaquin Valley and other advances in the community velocity model, in *2009 Southern California Earthquake Center Annual Meeting, Proceedings and Abstracts*, vol. 19, pp. 260–261.

Plesch, A., C. Tape, R. Graves, J. Shaw, P. Small, and G. Ely (2011), Updates for the CVM-H including new representations of the offshore Santa Maria and San Bernardino basins and a new Moho surface, in *2011 Southern California Earthquake Center Annual Meeting, Proceedings and Abstracts*, vol. 21, p. 214.

Sandwell, D., et al. (2010), Comparison of 16 strain rate maps for southern California, in *2010 Southern California Earthquake Center Annual Meeting, Proceedings and Abstracts*, vol. 20, p. 271.

Tape, C., Q. Liu, A. Maggi, and J. Tromp (2009a), Adjoint tomography of the southern California crust, *Science*, *325*, 988–992.

Tape, C., P. Musé, M. Simons, D. Dong, and F. Webb (2009b), Multiscale estimation of GPS velocity fields, *Geophys. J. Int.*, *179*, 945–971.

Tape, C., Q. Liu, A. Maggi, and J. Tromp (2009c), Adjoint tomography of the southern California crust, Eos Trans. Am. Geophys. Un., 90(52), Fall Meet. Suppl., Abstract S33B-2066.

Tape, C., Q. Liu, A. Maggi, and J. Tromp (2010a), Seismic tomography of the southern California crust based on spectral-element and adjoint methods, *Geophys. J. Int.*, *180*, 433–462.

Tape, C., A. Plesch, and J. H. Shaw (2010b), Expansion of CVM-H 6.2 to offshore and central California, in *2010 Southern California Earthquake Center Annual Meeting, Proceedings and Abstracts*, vol. 20, pp. 282–283.

Tape, C., Q. Liu, J. Tromp, A. Plesch, and J. H. Shaw (2010c), Time reversal seismic imaging using laterally reflected surface waves in southern California, in *2010 Southern California Earthquake Center Annual Meeting, Proceedings and Abstracts*, vol. 20, p. 282.

Tape, C., Q. Liu, J. Tromp, A. Plesch, and J. H. Shaw (2010d), Time reversal seismic imaging using laterally reflected surface waves in southern California, Abstract S44A-03 presented at 2010 Fall Meeting, AGU, San Francisco, Calif., 13-17 Dec.

Tape, C., J. P. Loveless, and B. J. Meade (2011a), Static displacements computed from seismic wavefield simulations: Validation tests for homogeneous and 1D structure, in *2011 Southern California Earthquake Center Annual Meeting, Proceedings and Abstracts*, vol. 21, p. 235.

Tape, C., E. Casarotti, A. Plesch, and J. H. Shaw (2011b), Seismogram-based assessment of the southern California seismic velocity model CVM-H 11.9 with 234 reference earthquakes, in *2011 Southern California Earthquake Center Annual Meeting, Proceedings and Abstracts*, vol. 21, p. 235.

Tape, C., A. Plesch, J. H. Shaw, and H. Gilbert (2012), Estimating a continuous Moho surface for the California Unified Velocity Model, *Seis. Res. Lett.* (in review).